

Searching for cosmic antihelium nuclei with the GAPS experiment

A. Stoessl^{a,*} on behalf of the GAPS Collaboration

(a complete list of authors can be found at the end of the proceedings)

^a*Departement of Physics and Astronomy,
University of Hawaii at Manoa,
2505 Correa Rd, Honolulu, HI 96822*

At low energies, cosmic antideuterons and antihelium provide an ultra-low background signature of dark matter annihilation, decay, and other beyond the Standard Model phenomena. The General Antiparticle Spectrometer (GAPS) is an Antarctic balloon experiment designed to search for low-energy (0.1–0.3 GeV/ n) antinuclei, and is planned to launch in the austral summer of 2022. While optimized for an antideuteron search, GAPS also has unprecedented capabilities for the detection of low-energy antihelium nuclei, utilizing a novel detection technique based on the formation, decay, and annihilation of exotic atoms. The AMS-02 collaboration has recently reported several antihelium nuclei candidate events, which sets GAPS in a unique position to set constraints on the cosmic antihelium flux in an energy region which is essentially free of astrophysical background. In this contribution, we illustrate the capabilities of GAPS to search for cosmic antihelium-3 utilizing complete instrument simulations, event reconstruction, and the inclusion of atmospheric effects. We show that GAPS is capable of setting unprecedented limits on the cosmic antihelium flux, opening a new window on exotic cosmic physics.

*37th International Cosmic Ray Conference (ICRC 2021)
July 12th – 23rd, 2021
Online – Berlin, Germany*

*Presenter

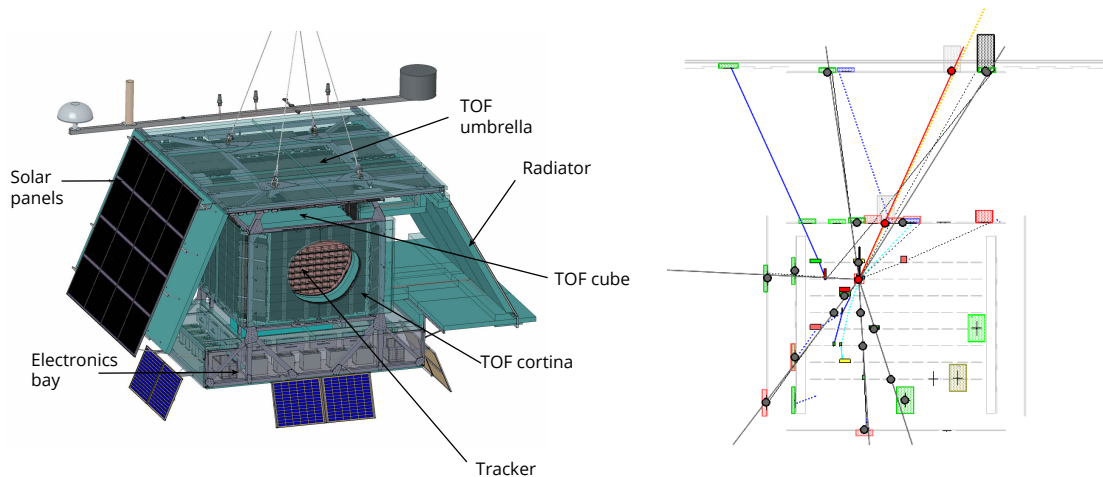


Figure 1: *Left:* A schematic overview of the GAPS instrument: The innermost detector component consists of 1000 Si(Li) detectors arranged in ten tracking planes (or layers), which is tightly encapsulated in a cube of plastic scintillator paddles which form the inner TOF system. The sides of the cube are enclosed in another layer of plastic scintillators ("cortina"), which together with the topmost layer ("umbrella") form the outer TOF system. *Right:* Topology of an antihelium-3 nucleus event, which passes all cuts. The red line denotes the incoming primary, while the gray lines are pions created in the annihilation, which is happening in the second uppermost layer of the Si(Li) tracker.

1. Introduction

The General Antiparticle Spectrometer (GAPS) is an indirect dark matter detection experiment optimized to detect low-energy ($0.1\text{--}0.3\text{ GeV}/n$) cosmic antiprotons, antideuterons, and antihelium using a series of Antarctic long-duration balloon (LDB) flights. Due to their ultra-low backgrounds, cosmic ray anti-nuclei heavier than antiprotons are excellent probes for dark matter models that predict dark matter annihilation or decay in the Galactic halo, including many models that evade detection in collider, direct, or other indirect searches [1]. BESS-Polar set an exclusion limit on the antihelium to helium flux ratio of $1.0 \cdot 10^{-7}$ in the range of $1.6\text{--}14\text{ GV}$ [2]. This is the most stringent upper limit on the antihelium flux prior to the tantalizing AMS-02 reports of the observation of several high-momenta ($>10\text{ GeV}/c$) candidate antihelium-3 and antihelium-4 nuclei events [3]. The analysis and interpretation of these events is ongoing. GAPS probes the low-energy region nearly inaccessible to AMS-02 due to the geomagnetic cutoff, with an orthogonal technique.

This work presents an update on the GAPS antihelium-3 sensitivity studies [4], including a slightly modified detector geometry, optimized to achieve to goal of a long-distance flight as well as an improved event reconstruction [5].

2. The GAPS experiment

2.1 Instrument overview

The GAPS experiment is designed to detect cosmic antinuclei during a series of LDB flights at high-altitude ($\approx 37\text{ km}$) above Antarctica. As shown in Fig.1, the instrument has two different detector components, the innermost being a particle tracker. It is formed from 1000 10 cm diameter,

2.5 mm thick lithium-drifted silicon (Si(Li)) detectors, arranged into ten tracking planes. Each Si(Li) detector has a cylindrical geometry with an active area of about 70 cm^2 that is segmented into eight single-sided strips of equal area [6–9]. The energy resolution of these detectors is close to 4 keV in the 20–100 keV range, and the electronics provide a high dynamic range for measuring particle tracks with individual energy depositions up to 100 MeV before saturation. A novel, oscillating heat pipe system [10] in conjunction with a rotator to keep the radiator pointed away from the Sun is used to cool the Si(Li) detectors to the requisite operational temperature ($\approx -40 \text{ }^\circ\text{C}$).

The entire tracker is encapsulated by a time-of-flight (TOF) system (Fig. 1). The TOF system in its current design consists of 160 plastic scintillator paddles. Each plastic scintillator paddle is 6.35 mm thick and 16 cm wide. The TOF is arranged into two subsystems. The inner TOF ("cube") encloses all six sides of the tracker system. The outer TOF is comprised of a planar layer called the "umbrella" that is centered over the cube at a minimum distance of 90 cm, and a second layer called the "cortina" that surrounds the sides of the cube at a minimum distance of 30 cm. The umbrella in combination with the top face of the cube is optimized to provide a trigger decision for incoming primaries and enables a precise measurement of secondary velocities while the cortina allows to measure the velocity of secondaries, whereas being lightweight enough to fulfill the strong weight constraints for the balloon payload. Currently, the TOF design is under review, as well as the trigger design. The sideways facing cortina is part of the trigger system as well.

3. Generated dataset

A more detailed description of the simulation procedure can be found in [4]. For these proceedings, the simulation has been updated to use the latest version of Geant4 Geant4v10.7.p02. In contrast to [4] the design of the TOF system has been altered in the simulation, to reflect current changes in the design. The effect of the utilization of the exotic X-ray lines is currently under study, and not part of this analysis. For the study presented here, we generated 10^{11} protons, $4 \cdot 10^9$ α -particles as well as $7 \cdot 10^8$ antiprotons.

4. Particle identification

The GAPS reconstruction algorithm focuses on reconstructing the primary track utilizing the timestamps from the TOF system. The reconstructed primary track is then extrapolated into the tracker system and tracker hits are iteratively added if they are spatially and energetically consistent. In the case that a primary track has been identified, a search for the annihilation star is performed. Secondary tracks are fitted to be consistent with late hits found in the TOF, also providing a reconstructed time for the annihilation. The GAPS reconstruction algorithm has been discussed in detail in [5].

The event selection is performed in two stages: in a first preselection, event quality is ensured by removing events which do not have their reconstructed annihilation star, or stopping point, within the volume of the Si(Li) tracker. Further, we require one hit from the reconstructed primary track in each of the TOF systems, outer and inner, as well as no more than a single active volume on the reconstructed track without hits. The second stage of the analysis focuses on the suppression of

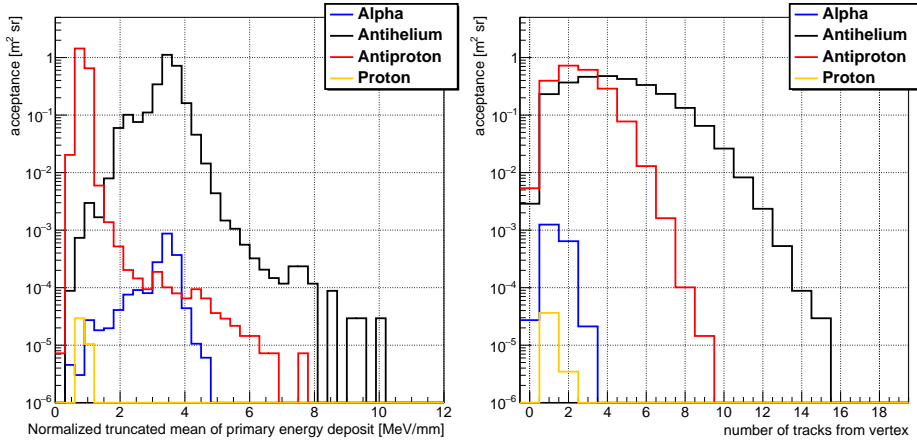


Figure 2: Two of the 7 variables which make up the second stage of the event selection. The normalized truncated mean of the energy deposition of the primary on the left, and the number of secondary tracks from the annihilation on the right. The truncated mean allows the separation of charge $|Z| = 1$ and $|Z| = 2$ particles. The number of secondary tracks separates particles and antiparticles, since the first category typically does not exhibit an annihilation star event pattern. It also allows to separate different nuclei masses. The distributions are shown after applying the preselection criteria to ensure all events have well-defined stopping vertices within the tracker volume. The distributions are slices from the generated 2d probability distributions, taken for the slice $0.39 < \beta < 0.41$

antiprotons, as well as remaining α . A detailed description of the variables can be found in [4]. In short, the variables used can be divided into two groups:

Classification of the primary track: The pattern of the energy depositions along the primary track has strong separation power especially against $|Z| = 1$ particles since the energy loss increases quadratically with charge. To disentangle the true ionization loss of the primary from the annihilation and other secondary energy depositions, it has been found that a **truncated mean of the energy depositions** has the largest separation power. The **primary column density** on the other hand describes the grammage traversed by the primary before stopping and exploits the fact that for the same velocity, antihelium-3 nuclei will typically traverse 25% less grammage than antiprotons, protons, and α -particles before they stop.

Classification of the annihilation star: The exact topology of the annihilation star depends on the particle as well. In general, heavier nuclei exhibit more secondary pions with higher energy. This fact is exploited with five variables: The **number of secondary tracks** and the **total number of hits** which reflect the fact of higher secondary multiplicity for heavier antinuclei as well as the **total energy deposition**, the **average velocity of secondary tracks** and the **Isotropy of secondary tracks**. The latter is exploiting the fact that with increasing velocity of the secondaries, the direction of their emission becomes boosted when approaching the speed of light. Two of these variables are shown in Fig.2

The event sample after the preselection cuts is then used to obtain 2d probability distributions for the seven variables in combination with the primary velocity. Atmospheric effects are taken into account by a separate set of simulations, as further described in [4]. The analysis has been performed for three equally large $\cos(\theta)$ ranges. For each angular range, the probability distributions were

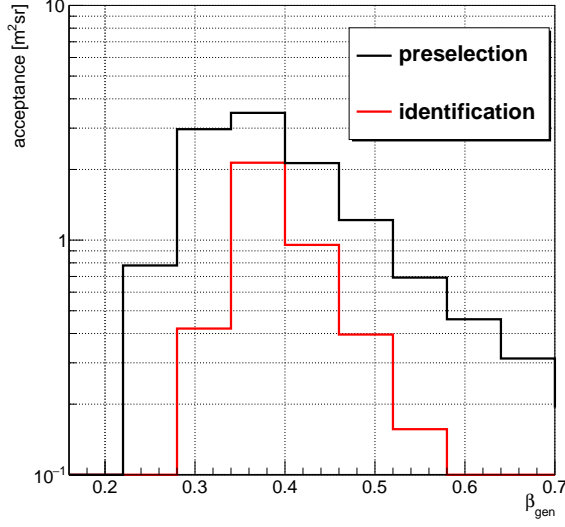


Figure 3: The GAPS acceptance as a function of generated β as calculated for the top of the instrument for antihelium-3 nuclei after the two stages of the event selection.

calculated for each particle species, and then finally a likelihood value \mathcal{L} expressing the likeliness of the primary being member of each of these species was calculated. The ratio L of $\mathcal{L}_{\text{He}^3}$ over the sum of the likelihood value of all species then reflects the probability of an event being an antihelium-3 event. Cuts on $-\ln(L)$ were optimized to reject background events while maximizing GAPS's antihelium-3 nuclei acceptance for each of the three angular bins individually. The cuts have been chosen such that one detected antihelium-3 nucleus provides an unambiguous discovery. Two further cuts were applied in the final stage of the analysis. Candidate antihelium-3 nucleus events are required to have a truncated mean energy deposition corresponding to a charge of $|Z| = 2$ particle, to ensure an unambiguous charge measurement of the primary. Furthermore, candidate events are required to have a reconstructed velocity β in the range of 0.3–0.6 to assure that a candidate antihelium-3 nucleus could stop inside the TOF cube [4]. Fig. 3 compares the acceptance for antihelium-3 nuclei of both stages of the event selection. The antihelium-3 nuclei identification efficiency is at the level of about 50% for the peak region around $\beta \approx 0.34 - 0.52$. To estimate the number of background events passing cuts, the background acceptances after all identification cuts are integrated with the background fluxes. For a more detailed description of the impact of atmospheric effects on the background and signal fluxes, we have to refer to [4] as well as an upcoming publication on atmospheric effects.

5. Sensitivity estimate

The number of remaining background events b in the final sample is on the order of about 10^{-3} for one LDB flight of 35 days. Following a Bayesian approach as in [19] we calculate the antihelium-3 flux sensitivity S as follows.

$$S = \frac{n - b}{\bar{A}_{\text{id}} T \Delta E \epsilon_{\text{geo}} \epsilon_s}. \quad (1)$$

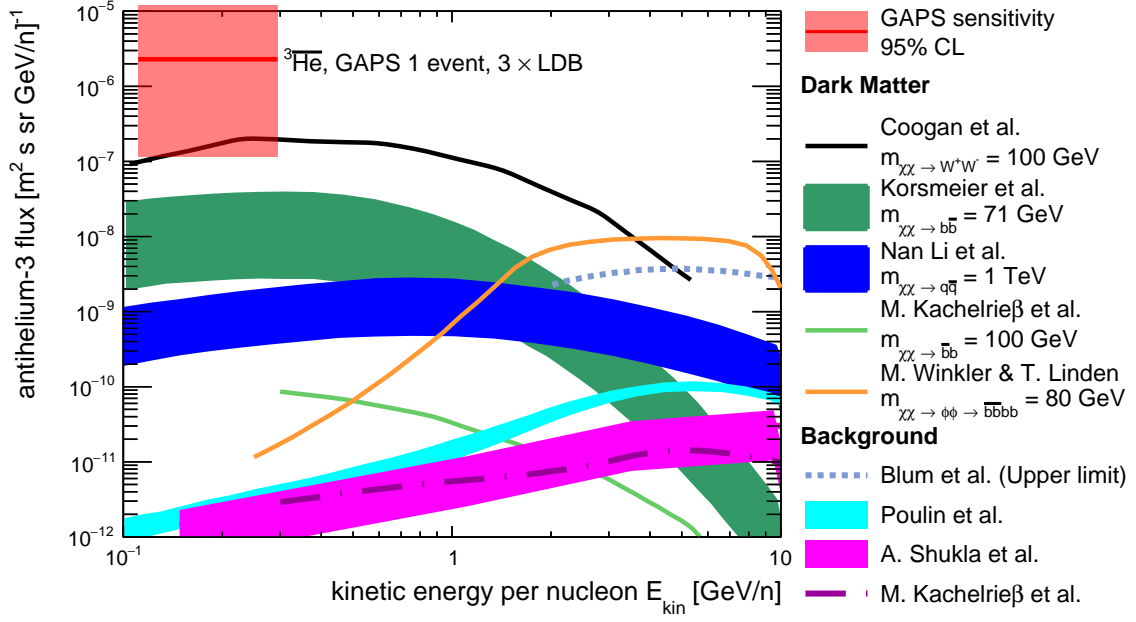


Figure 4: The solid red line shows the single event sensitivity of GAPS to antihelium-3 nuclei (95% confidence level) for three LDB flights of 35 days each. The red box indicates the upper and lower bounds of the 95% confidence level. Also shown are the antihelium-3 flux predicted by a variety of dark matter [11–15] and standard astrophysical background [16–18] models. For theoretical predictions, the error bands illustrate uncertainties in the coalescence momentum, but also include propagation uncertainties.

Here, T is the observation time (three 35-day LDB flights = 105 days). \bar{A}_{id} is the average antihelium-3 nuclei identification acceptance in the kinetic energy range of 0.11–0.3 GeV/ n , ϵ_{geo} is the geomagnetic cutoff efficiency for antihelium-3 nuclei [20]. ϵ_s is the atmospheric survival probability for antihelium-3 nuclei, which describes the probability of an antihelium-3 nucleus to traverse the atmosphere without being absorbed. For three 35-day LDB flights, the projected GAPS antihelium-3 nuclei sensitivity is $2.29^{+7.8}_{-2.2} \cdot 10^{-6} \text{ m}^{-2} \text{ sr}^{-1} \text{ s}^{-1} (\text{GeV}/n)^{-1}$ (95% confidence level). The uncertainties in the projected sensitivities are estimated using the upper and lower limits of true antihelium-3 nuclei detections from the 95% confidence interval, based on the calculated mean number of background events. Fig. 4 shows the three-flight sensitivity in comparison with antihelium-3 fluxes predicted by a variety of dark matter [11–15] and astrophysical background [16–18] models. Within the 95% confidence interval, three GAPS flights have the potential to discover dark matter models annihilating into W^+W^- [12].

6. Conclusion

In these proceedings, we demonstrate that based on our current best estimate for the simulation of the instrument, event reconstruction, and consideration of atmospheric influence the GAPS experiment can achieve a sensitivity of $\pm \cdot 10^{-6} \text{ m}^{-2} \text{ sr}^{-1} \text{ s}^{-1} (\text{GeV}/n)^{-1}$ (95% confidence level) in the energy range of 0.11–0.3 GeV/ n for three 35-day LDB flights. This is compatible with our result in [4], despite the design changes in the outer TOF system. This sensitivity extends to lower energies than any previous experiment, complementing the exclusion limits set by BESS-Polar and ongoing

searches with AMS-02. Due to its orthogonal systematic uncertainties and sensitivity to the lower-energy range, where the predicted contribution from new-physics models is highest, GAPS will provide crucial input to interpret the AMS-02 candidate events.

7. Acknowledgments

This work is supported in the U.S. by NASA APRA grants (NNX17AB44G, NNX17AB45G, NNX17AB46G, and NNX17AB47G), in Japan by JAXA/ISAS Small Science Program FY2017, and in Italy by Istituto Nazionale di Fisica Nucleare (INFN) and the Italian Space Agency through ASI INFN agreement No. 2018-28-HH.0: “Partecipazione italiana al GAPS - General AntiParticle Spectrometer”. F. Rogers is supported by the National Science Foundation Graduate Research Fellowship under Grant No. 1122374. P. von Doetinchem received support from the National Science Foundation under award PHY-1551980. H. Fuke is supported by JSPS KAKENHI grants (JP17H01136 and JP19H05198) and Mitsubishi Foundation Research Grant 2019-10038. K. Perez and M. Xiao are supported by Heising-Simons award 2018-0766. Y. Shimizu receives support from JSPS KAKENHI grant JP20K04002 and Sumitomo Foundation Grant No. 180322. Technical support and advanced computing resources from the University of Hawaii Information Technology Services – Cyberinfrastructure are gratefully acknowledged. This research was done using resources provided by the Open Science Grid [21, 22], which is supported by the National Science Foundation award #2030508.

References

- [1] P.v. Doetinchem et al., *Journal of Cosmology and Astroparticle Physics* **2020** (2020) 035.
- [2] K. Abe et al., *Phys. Rev. Lett.* **108** (2012) 131301.
- [3] S. Ting, *Press Conference at CERN, December 8* (2016) .
- [4] N. Saffold, T. Aramaki, R. Bird, M. Boezio, S. Boggs, V. Bonvicini et al., *Astroparticle Physics* **130** (2021) 102580.
- [5] R. Munini, E. Vannuccini, R. Bird, M. Boezio, P. von Doetinchem, C. Gerrity et al., *publication under review* (2021) .
- [6] K. Perez et al., *Nucl. Instrum. Meth. A* **905** (2018) 12 [1807.07912].
- [7] M. Kozai et al., *Nucl. Instrum. Meth. A* **947** (2019) 2695 [1906.05577].
- [8] F. Rogers et al., *Journal of Instrumentation* **14** (2019) P10009.
- [9] N. Saffold et al., *Nucl. Instrum. Meth. A* **997** (2021) 165015.
- [10] S. Okazaki et al., *Applied Thermal Engineering* **141** (2018) 20 .
- [11] M. Korsmeier, F. Donato and N. Fornengo, *Physical Review D* **97** (2018) 103011.
- [12] A. Coogan and S. Profumo, *Physical Review D* **96** (2017) 083020.

- [13] K. Blum et al., *Physical Review D* **96** (2017) .
- [14] Y.-C. Ding et al., *Journal of Cosmology and Astroparticle Physics* **2019** (2019) 004.
- [15] M.W. Winkler and T. Linden, *Physical Review Letters* **126** (2021) .
- [16] V. Poulin et al., *Physical Review D* **99** (2019) 023016 [1808.08961].
- [17] M. Kachelrieß, S. Ostapchenko and J. Tjemsland, *Journal of Cosmology and Astroparticle Physics* **2020** (2020) 048.
- [18] A. Shukla et al., *Physical Review D* **102** (2020) 063004.
- [19] G.J. Feldman and R.D. Cousins, *Physical Review D* **57** (1998) 3873.
- [20] P. Doetinchem and B. Yamashiro, *PoS ICRC2017* (2017) 151.
- [21] R. Pordes, D. Petravick, B. Kramer, D. Olson, M. Livny, A. Roy et al., *The open science grid*, in *J. Phys. Conf. Ser.*, vol. 78 of 78, p. 012057, 2007, DOI.
- [22] I. Sfiligoi, D.C. Bradley, B. Holzman, P. Mhashilkar, S. Padhi and F. Wurthwein, *The pilot way to grid resources using glideinwms*, in *2009 WRI World Congress on Computer Science and Information Engineering*, vol. 2 of 2, pp. 428–432, 2009, DOI.

Full Authors List: GAPS Collaboration

T. Aramaki¹, R. Bird², M. Boezio^{3,4}, S. E. Boggs⁵, V. Bonvicini³, D. Campana⁶, W. W. Craig⁷, E. Everson², L. Fabris⁸, H. Fuke⁹, F. Gahbauer¹⁰, I. Garcia², C. Gerrity¹¹, C. J. Hailey¹⁰, T. Hayashi², C. Kato¹², A. Kawachi¹³, S. Kobayashi¹³, M. Kozai⁹, A. Lenni^{3,14}, A. Lowell⁷, M. Manghisoni^{15,16}, N. Marcelli^{17,18}, S. A. I. Mognet¹⁹, K. Munakata¹², R. Munini^{3,4}, Y. Nakagami²⁰, J. Olson²¹, R. A. Ong², G. Osteria⁶, K. Perez²², S. Quinn², V. Re^{15,16}, E. Riceputi^{15,16}, B. Roach²², F. Rogers²², J. A. Ryan², N. Saffold¹⁰, V. Scotti^{6,23}, Y. Shimizu²⁴, M. Sonzogni^{15,16}, R. Sparvoli^{17,18}, A. Stoessl¹¹, A. Tiberio²⁵, E. Vannuccini²⁵, P. von Doetinchem¹¹, T. Wada²⁰, M. Xiao²², M. Yamatami⁹, A. Yoshida²⁰, T. Yoshida⁹, G. Zampa³, and J. Zweerink²

¹Northeastern University, 360 Huntington Avenue, Boston, MA 02115, USA. ²University of California, Los Angeles, Los Angeles, CA 90095, USA. ³INFN, Sezione di Trieste, I-34149 Trieste, Italy. ⁴IFPU, I-34014 Trieste, Italy. ⁵University of California, San Diego, La Jolla, CA 90037, USA. ⁶INFN, Sezione di Napoli, I-80126 Naples, Italy. ⁷Space Sciences Laboratory, University of California, Berkeley, 7 Gauss Way, Berkeley, CA 94720, USA. ⁸Oak Ridge National Laboratory, Oak Ridge, TN 37831, USA. ⁹Institute of Space and Astronautical Science, Japan Aerospace Exploration Agency (ISAS/JAXA), Sagamihara, Kanagawa 252-5210, Japan. ¹⁰Columbia University, New York, NY 10027, USA. ¹¹University of Hawaii at Manoa, Honolulu, HI 96822 USA. ¹²Shinshu University, Matsumoto, Nagano 390-8621, Japan. ¹³Tokai University, Hiratsuka, Kanagawa 259-1292, Japan. ¹⁴Università di Trieste, I-34127 Trieste, Italy. ¹⁵INFN, Sezione di Pavia, I-27100 Pavia, Italy. ¹⁶Università di Bergamo, I-24044 Dalmine (BG), Italy. ¹⁷INFN, Sezione di Rome "Tor Vergata", I-00133 Rome, Italy. ¹⁸Università di Roma "Tor Vergata", I-00133 Rome, Italy. ¹⁹Pennsylvania State University, University Park, PA 16802 USA. ²⁰Aoyama Gakuin University, Sagamihara, Kanagawa 252-5258, Japan. ²¹Heliospace Corporation, Berkeley, CA 94710, USA. ²²Massachusetts Institute of Technology, Cambridge, MA 02139, USA. ²³Università di Napoli "Federico II", I-80138 Naples, Italy. ²⁴Kanagawa University, Yokohama, Kanagawa 221-8686, Japan. ²⁵INFN, Sezione di Firenze, I-50019 Sesto Fiorentino, Florence, Italy.

Web version: gaps1.astro.ucla.edu/gaps/authors/